ARTICLE

Hydrothermal Synthesis of $Li_9Fe_3(P_2O_7)_3(PO_4)_2$ Nanoparticles and Their Photocatalytic Properties under Visible-Light Illumination

Fei Ji, Chaolin Li,* and Jiahuan Zhang

Environmental Science & Engineering Research Center, Shenzhen Graduate School, Harbin Institute of Technology, Shenzhen 518055, P. R. China

ABSTRACT A visible-light-driven photocatalyst, $Li_9Fe_3(P_2O_7)_3(PO_4)_2$, prepared by a hydrothermal method was studied. The as-prepared catalyst exhibited efficient photocatalytic activity in the degradation of methylene blue (MB) under visible-light irradiation ($\lambda > 400$ nm). Besides decoloring, the decomposition of phenol was also observed, further demonstrating the photocatalytic performance of $Li_9Fe_3(P_2O_7)_3(PO_4)_2$. It was found that hexadecyltrimethylammonium bromide (CTAB) affected the geometry, crystallinity, optical property, surface area, and photocatalytic activity of the material significantly. The sample obtained with CTAB addition during synthesis procedure showed the higher photocatalytic activity. 70% of MB could be photodegraded under visible-light irradiation after 3 h, showing the excellent photocatalytic activity of $Li_9Fe_3(P_2O_7)_3(PO_4)_2$. Furthermore, with I^- as electron donor, 19 umol/g of hydrogen was photocatalytically evolved from aqueous solutions after 5 h. According to experimental results, a possible photocatalytic mechanism of $Li_9Fe_3(P_2O_7)_3(PO_4)_2$ was proposed.

KEYWORDS: photocatalyst • phosphate • degradation • water splitting • visible light

1. INTRODUCTION

Semiconductor photocatalysis has been the focus of much research for its application in splitting water to supply clean, recyclable hydrogen energy and for decomposing organic contaminants (1−3). TiO_2 has been widely used as an effective and inexpensive photocatalyst (4). However, TiO_2 is only active in the ultraviolet (UV) light range (5). It has been of great interest to develop highly active photocatalysts that work efficiently under visible-light irradiation. Modification of TiO_2 by doping or dye-sensitization has been intensely studied to exploit the photocatalyst response to visible-light irradiation (6−9). However, doped materials often suffer from thermal instability (10), and many dye sensitizers are not sufficiently stable in the aquatic environment (11). To eliminate these drawbacks, a large number of investigations have focused on undoped, single-phase oxide photocatalysts working under visible-light illumination (12−14). However, the metal elements of many new catalysts are rare, and the visible-light-driven photocatalysts are usually synthesized by high-temperature ceramic methods, which are characterized by high energy consumption. Therefore, it is of great importance to develop easily prepared, earth-abundant photocatalysts.

It was reported that some phosphates exhibited photoluminescence properties (15). Considering some photocatalysts also have photoluminescence properties (16, 17), the phosphates may have potential application in photocatalyst. In addition to P, Fe is also an abundant element, which is commonly used to make various catalysts (18, 19). Therefore, we think that a combination of P and Fe might develop a new photocatalyst.

$Li_9Fe_3(P_2O_7)_3(PO_4)_2$ was previously synthesized by high-temperature ceramic method and reported as one of the several monodiphosphates (20). Recently, we prepared this material by hydrothermal method. Its good visible-light absorption ability indicated that it may be a photocatalyst working under visible light. In the present paper, we report the synthesis of $Li_9Fe_3(P_2O_7)_3(PO_4)_2$ nanoparticles and their photocatalytic properties. Our method of synthesis was characterized by low temperature and short time. The as-prepared photocatalysts exhibited good visible-light absorption and high photocatalytic activity. Photocatalytic decomposition of water to produce hydrogen over the catalyst was also observed.

2. EXPERIMENTAL SECTION

2.1. Sample Preparation. Photocatalysts were prepared by a hydrothermal method. All chemicals are of analytic purity and used without further purification. In a typical procedure, the CTAB was dissolved in 50 mL H_3PO_4 solution (0.1 mol L^{-1}). Sixty-three hundreths of a gram of of $LiOH \cdot H_2O$ and 1.39 g of $FeSO_4 \cdot 7H_2O$ powders were added to the solution. The solution was quickly transferred to a Teflon-lined stainless steel autoclave (inner volume: 120 mL) and heated at 150 °C for 2 h. After the hydrothermal reaction, the reactor was cooled to room temperature. The precipitated powder was washed with ethanol to ensure elimination of the excess of surfactant. Then, the obtained powder was dried at 50 °C under a vacuum. For comparison, the catalyst without CTAB addition during synthesis was also prepared by the same procedure. The two samples obtained in this manner are hereafter named SA (sample obtained in the absence of CTAB during synthesis) and SB

* Corresponding author. Tel./Fax: +86 755 26032455. E-mail: lichaolin@hitsz.edu.cn.

Received for review March 6, 2010 and accepted May 12, 2010

DOI: 10.1021/am100189m

Published on Web 05/20/2010

(sample obtained in the presence of CTAB during synthesis). A common visible-light-responsive photocatalyst N-doped TiO_2 was synthesized (21). The N-doped TiO_2 and a commercial TiO_2 photocatalyst (Degussa P25) were used as reference photocatalyst.

2.2. Characterization. The phase compositions of the as-prepared samples were characterized by X-ray diffraction (XRD) on a Japan Rigaku D/max 2500 PC diffractometer using Cu Ka radiation. Scanning electron microscopy (SEM) characterizations were performed on a Hitachi S-4700 electron probe microanalyzer. The UV−visible diffuse reflectance spectra (DRS) of the samples were measured using a Shimadzu UV-2450 UV−visible spectrophotometer with barium sulfate as the reference sample. The Brunauer−Emmett−Teller (BET) surface area measurements were performed by a Micromeritics ASAP2020 surface area analyzer.

2.3. Photocatalytic Activity Test. The photocatalytic activities of the samples were evaluated by degradation of MB and phenol in an aqueous solution under visible light from a 350 W xenon lamp. The light below 400 nm was removed by using a glass filter. In each test, 50 mg of the photocatalyst was dispersed in 10 mg L^{-1} MB or phenol solution (100 mL). The reaction temperature was controlled at 25 °C by a circulating water jacket. Prior to irradiation, the suspension was magnetically stirred in dark for about 30 min to reach absorption−desorption equilibrium. The suspension was kept under constant air-equilibrated conditions during illumination. At certain time intervals, 5 mL suspension was sampled and centrifuged to remove the particles. The degradation of MB was monitored by a Hitachi U-3010 UV−vis spectrophotometer at 665 nm. The concentration of phenol was determined by using a colorimetric assay (22). Photocatalytic splitting of water to hydrogen was carried out in a Pyrex reactor of 250 cm^3 capacity. In a typical reaction, 0.1 g of catalyst was added to 100 mL of aqueous solution of 0.2 M KI in the Pyrex reactor (23). The mixture was suspended by using a magnetic stirrer within the reactor. Prior to the reaction, the mixture was deaerated by evacuation and then flushed with N_2 repeatedly to remove O_2 and CO_2 dissolving in water. The light below 400 nm was also removed by using a glass filter. The reactor was irradiated using a 350 W xenon lamp after gas chromatography (GC) analysis confirmed that the amount of air in the reactor was negligible. The reaction was carried out and the reaction products were analyzed by GC (Shimadzu 2014 C system, a molecular sieve 5 A column, a thermal conductivity detector, and N_2 as the carrier gas) at intervals of 1 h. To check the reproducibility of catalyst, the resulting suspension was centrifugalized at the end of experiment. The separated catalyst was reused for repeated tests.

The measurements were repeated for each catalyst and the results were reproducible within the experiments errors (±3%).

3. RESULTS AND DISCUSSION

3.1. Catalyst Characterization. It was reported that geometry is an important factor affecting activity of photocatalyst. With similar particle surface areas, a different geometry results in a different efficiency of photocatalytic degradation (24). The morphological characteristic of the two samples were first investigated by SEM. The morphology of the sample SA, as shown in Figure 1a, was blocky and the particle size was in the rage of 500−1000 nm. As shown in Figure 1b, the morphology of the sample SB exhibited a rodlike morphology, where the length and diameter of the rods varied over the ranges of 500−1000 and 100−200 nm, respectively. The growth pattern of nanocrystals could be influenced by the surfactants such as CTAB and dodecyl benzene sulfonic acid sodium (DBS) (25−28). With the existence of CTAB, the energy between solution and the crystal was reduced, and the crystal favored to grow preferentially along the direction that the CTAB absorbed (29). Morphologies of the samples obtained with different amount of CTAB addition were shown in Figure S2 of the Supporting Information. The results clearly show that the CTAB is responsible for the formation of nanorods in large quantities.

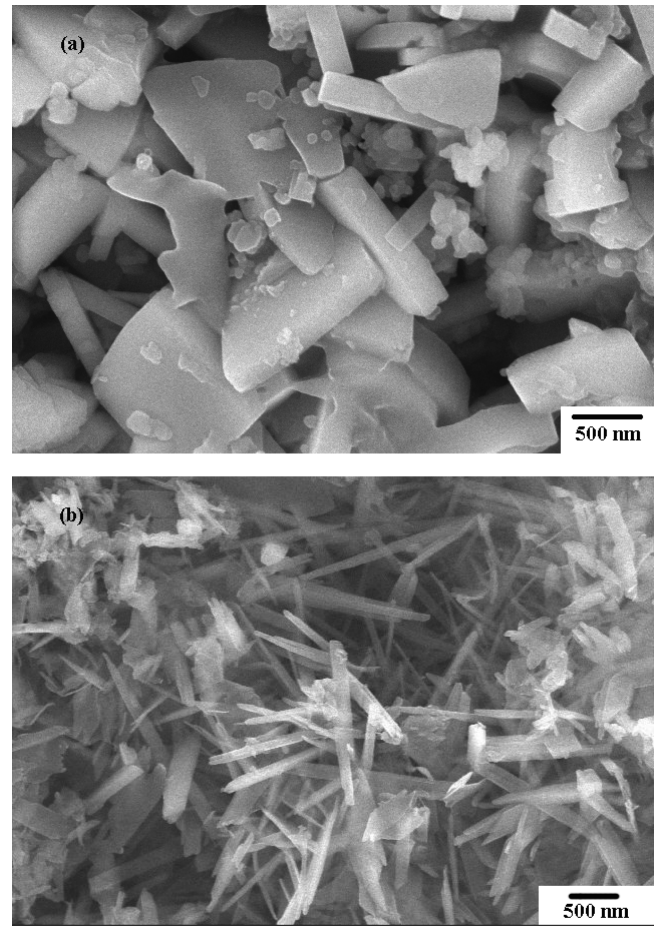

FIGURE 1. Scanning electron micrographs of (a) sample SA and (b) sample SB.

The XRD patterns of the sample SA is shown in Figure 2a. The peaks of the samples match well with PDF 01−089−4707. The main diffraction peaks can be attributed to the phase of $Li_9Fe_3(P_2O_7)_3(PO_4)_2$. The cell constants of the sample SA was calculated to be $a = 9.75$ Å, $b = 9.75$ Å, and $c = 13.37$ Å, which differ slightly from the PDF 01−089−4707 ($a = 9.72$ Å, $b = 9.72$ Å, and $c = 13.5$ Å). Figure 2b shows that the phase of catalyst is not changed during the heating process in the presence of CTAB. One notable observation from Figure 2b is that the intensity of the (002) peak decreases drastically relative to those of the other peaks. Such changes could be attributed to preferential orientation of the crystal. Different geometries of these different samples also support this view.

It is widely accepted that the surface area of a photocatalyst greatly affect its catalytic activity (30). With greater surface area, the adsorbed molecules might be able to diffuse more rapidly at the surface of the catalyst, causing the photoreactions to carry on more easily. The surface area was 16 and 32.2 $m^2 g^{-1}$ for the sample SA and SB, respectively.

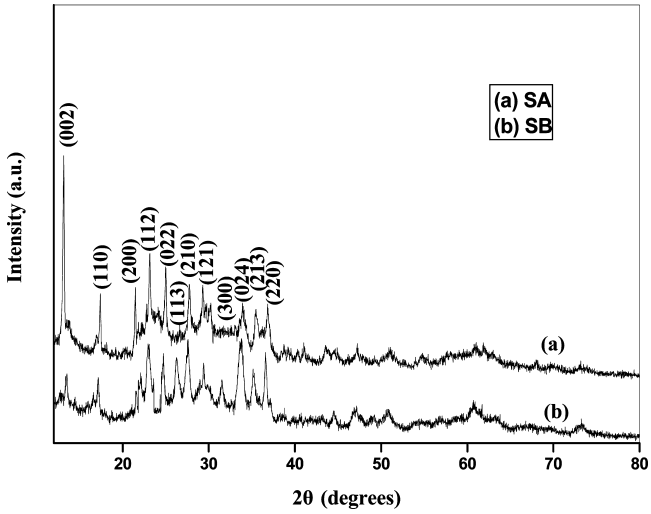

FIGURE 2. XRD patterns of the nanoparticles: (a) synthesized without CTAB; (b) synthesized with CTAB.

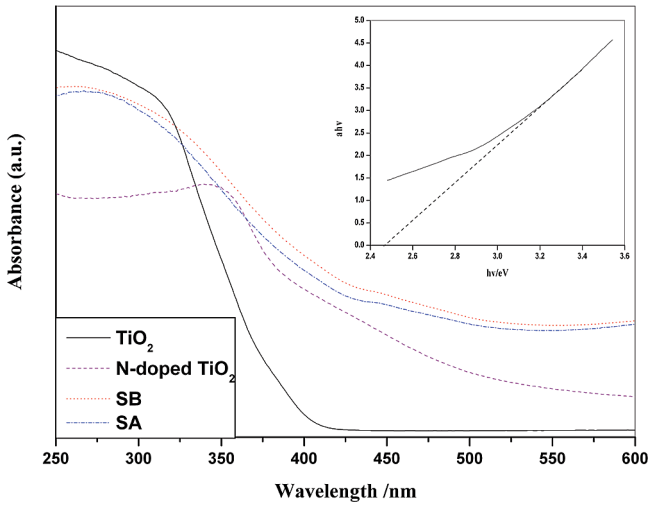

FIGURE 3. UV−vis absorption spectra of TiO_2, N-doped TiO_2 and $Li_9Fe_3(P_2O_7)_3(PO_4)_2$ samples, with the band gap E_g of sample SB (inset).

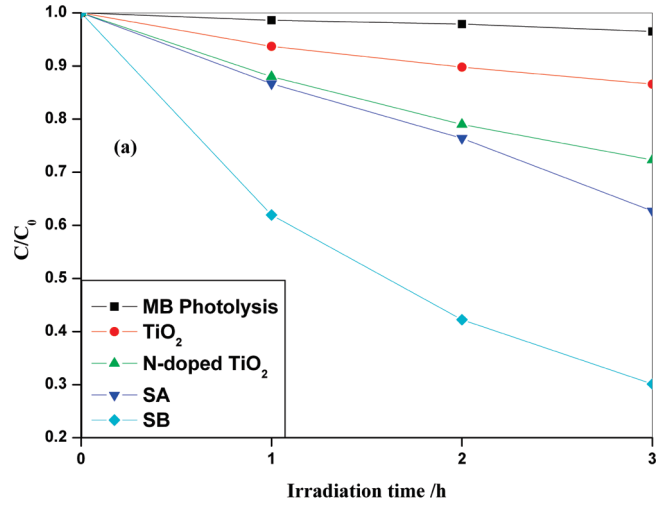

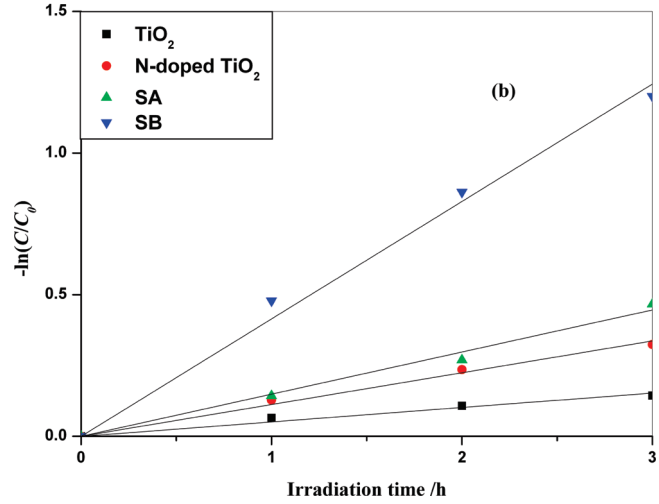

FIGURE 4. (a) Photodegradation efficiencies of MB (10 mg L^{-1}) as a function of irradiation time by different photocatalysts (catalyst, 0.5 g L^{-1}). (b) Kinetic linear simulation curve of MB photocatalytic degradation with different photocatalysts.

The large surface area of the sample SB may play important roles in its photocatalytic reaction.

The diffuse-reflection spectra of TiO_2, N-doped TiO_2, and the $Li_9Fe_3(P_2O_7)_3(PO_4)_2$ samples are depicted in Figure 3. The TiO_2 sample shows no absorption in the visible region with its band gap transition starting from 380 nm. A considerable shift of absorption edge to the visible-light region can be observed for the N-doped TiO_2 in comparison with TiO_2, which can be attributed to the nitrogen doping. Unlike the TiO_2, the $Li_9Fe_3(P_2O_7)_3(PO_4)_2$ samples have photoabsorption from UV light to visible light. The sample SA showed an absorption edge around 490 nm. The sample SB exhibited a greater light attenuation, and its absorption edge was slightly extended toward the visible-light range. There is a close relationship between the photoabsorption ability and the particle size. Similar red shift of absorption has also been observed for Cu_2O nanopaticles with different particle sizes (24).

3.2. Photocatalytic Performances. The photocatalytic activities of the as-prepared nanoparticles were evaluated by analyzing the photodegradation of methylene blue under visible-light irradiation. Figure 4a shows that illumination with visible light can lead to only about 5% decomposition of MB molecules after 3 h in the absence of any photocatalysts. To prove the UV light was cut off by the glass, the photocatalytic property of TiO_2 was also tested. Slight degradation of MB was observed in the presence of the photocatalyst P25 after 3 h under visible-light irradiation. This can be accounted for the photosensitized capability of MB molecules (31). The N-doped TiO_2 nanoparticles exhibited about 26% degradation rate of MB within 3 h. Under the same conditions, 70% of MB can be photodegraded by the sample SB while that by SA was 38%. Results showed that the excellent photocatalytic activity of the sample SB under visible-light irradiation. The higher degradation activity of the sample SB was mainly attributed to their high surface area and photoabsorption in the visible region.

A kinetic curve of MB photocatalytic degradation based on the data plotted in Figure 4a is shown in Figure 4b. It is obvious that the curve is close to a linear curve, which indicates the photocatalytic degradation of MB using the as-

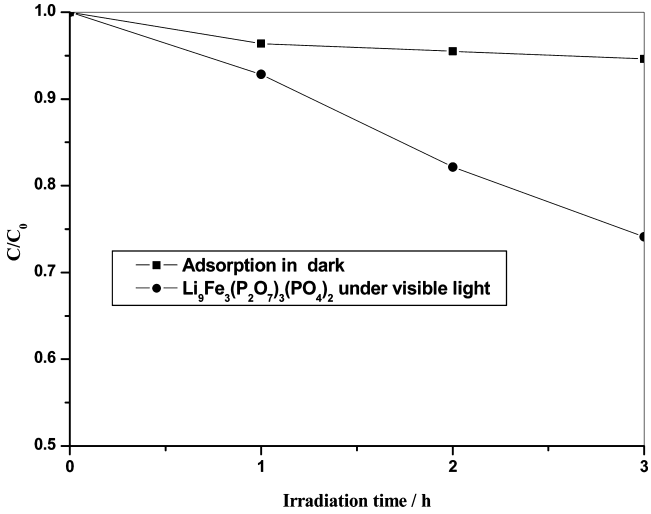

FIGURE 5. Photodegradation of phenol in the presence of sample SB under visible-light irradiation ($\lambda > 400$ nm).

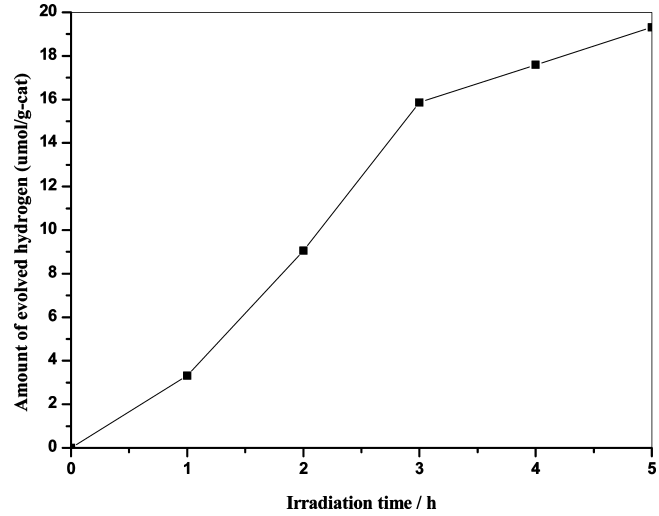

FIGURE 6. Photocatalytic hydrogen evolution activity of the sample SB as a function of irradiation time (catalyst, 1 g L^{-1}).

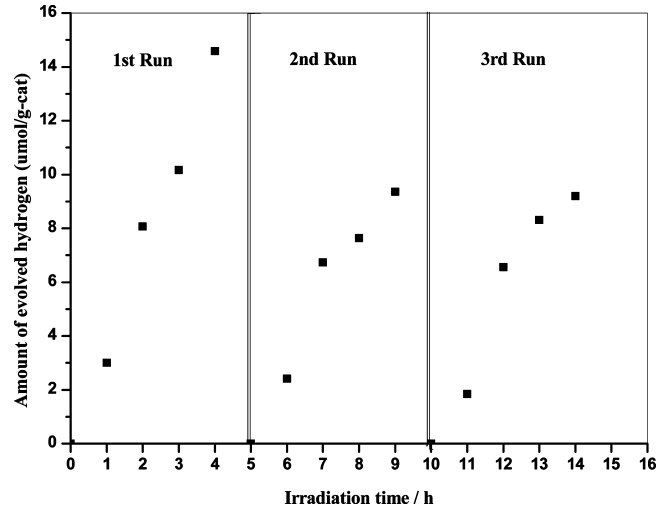

FIGURE 7. Photocatalytic hydrogen evolution experiments of the sample SB for three cycles.

prepared materials follows first-order reaction kinetics. The apparent reaction rate constant k for the sample TiO_2, N-doped TiO_2, SA, and SB was 0.0003, 0.0006, 0.0008, and 0.0023 min^{-1}, respectively, suggesting a preferable photocatalytic performance of the sample SB.

To further confirm the photocatalytic property of the as-prepared $Li_9Fe_3(P_2O_7)_3(PO_4)_2$, we selected phenol, which has no visible-light absorption, to evaluate the photocatalytic activity. As shown in Figure 5, it was found that phenol was degraded by the sample SB under visible-light irradiation. Twenty-six percent of phenol can be photodegraded after 3 h, and the adsorption of phenol on the sample SB in the dark was only 4%. Different from chemical dyes, phenol does not absorb visible light. Thus, the photosensitization process did not exist in such a photodegradation process. As a result, the degradation of phenol was fully attributed to the photocatalytic process, indicating that the $Li_9Fe_3(P_2O_7)_3(PO_4)_2$ is indeed a visible-light-induced photocatalyst.

Photocatalysts could be examined for degradation of water pollutants and water splitting for hydrogen evolution (32). Photocatalytic decomposition of water to produce hydrogen under visible-light irradiation over the photocatalyst was also investigated. I^- was used as a strong hole scavenger to reduce the recombination of the photoinduced electrons and holes (23). The result for hydrogen production as a function of irradiation time with the sample SB photocatalyst is shown in Figure 6. Visible-light irradiation of the aqueous $Li_9Fe_3(P_2O_7)_3(PO_4)_2$ suspension led to an apparent production of hydrogen. The amount of hydrogen evolution increases steadily with the irradiation time. After 5 h, the total hydrogen yield was 19.5umol g^{-1}. To evaluate the photostability of the as-prepared catalyst, producing hydrogen from the solution via photocatalysis was repeatedly studied for up to three cycles. The results are shown in Figure 7. The hydrogen yield after 4 h of visible-light irradiation was 15, 9.8, and 9.5 umol g^{-1}, respectively, for the three tests. A slight decrease in photoactivity after each cycle may be due to aggregation of nanoparticles during the catalytic process. The experimental results indicate that the catalyst has good reproducibility and can be used repeatedly with only a slight loss of activity for producing hydrogen.

3.3. Mechanism. As shown in Figure 3, the absorption edge of the sample SB is 500 nm. For a crystalline semiconductor, the optical band gap is determined by the following equation: $ah\nu = A(h\nu - E_g)^{2/n}$, where a, $h\nu$, A, and E_g are the absorption coefficient, light frequency, proportionality constant, and band gap, respectively (33). The values of n and E_g were determined using the published methods (34). As shown in Figure 3 (inset), the value of the band gap for the sample SB was estimated to be 2.53 eV.

We can calculate the conduction and valence band positions through the following empirical equation: $E_{CB} = X - E_e - 0.5E_g$, where X is the geometric mean of Mulliken's electronegativities of constituent atoms, E_e is the energy of free electrons on the hydrogen scale ($\approx$ 4.5 eV), and E_g is the band gap (35). Using calculations (shown in the Supporting Information), the conduction band (CB) edge position of the sample SB at the point of zero charge is evaluated at -0.445 eV (vs NHE). Correspondingly, the valence band (VB) potential is calculated at about 2.085 Ev (vs NHE).

Scheme 1. Proposed Mechanism of Photocatalytic Degradation of Organic Pollutants and Hydrogen Evolution over $Li_9Fe_3(P_2O_7)_3(PO_4)_2$

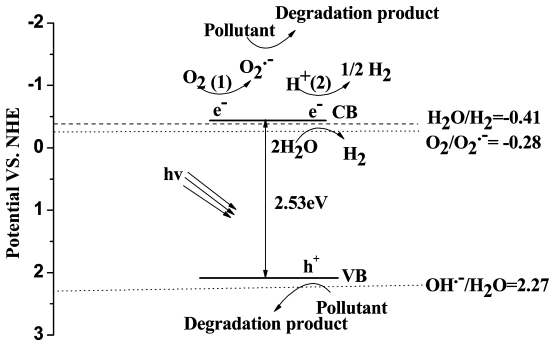

According to the above experimental results, a possible mechanism was proposed as shown in Scheme 1. Catalysts absorb light with energy higher than 2.53 eV and generate electron/hole pairs. For the proper conduction band position, it becomes more favorable for the electrons generated to react with adsorbed O_2, producing active radicals. The active radicals then react with pollutants through the pathway (36−38). As shown in Figure S2 of the Supporting Information, the decolorization efficiency of MB was remarkably decreased with N_2 purging, indicating that the oxygen played an important part in the photocatalytic process. The decolorization of MB in the absence of oxygen could be accounted for the reactions between the holes and the dye pollutants (39). For the hydrogen evolution in the absence of oxygen, the electrons in the conduction band of the particle will simultaneously reduce water or protons in the solution to form gaseous H_2 as the pathway (40).

4. CONCLUSIONS

In this work, photocatalytic removal of organic pollutants and decomposition of water to produce hydrogen under visible-light irradiation over the photocatalyst $Li_9Fe_3(P_2O_7)_3(PO_4)_2$ was studied. The results reported herein highlight a new area of exploration for the development of easily prepared, earth-abundant photocatalysts. It may provide useful information to further develop some effective phosphate catalysts for pollutant degradation under visible-light irradiation for water and wastewater treatment.

Supporting Information Available: Additional figures and calculations of E_{CB} (PDF). This material is available free of charge via the Internet at http://pubs.acs.org.

REFERENCES AND NOTES

(1) Wong, C. C.; Chu, W. *Environ. Sci. Technol.* **2003**, *37*, 2310.
(2) Zou, Z. G.; Ye, J. H.; Sayama, K.; Arakawa, H. *Nature* **2001**, *414*, 625.
(3) Gondal, M. A.; Sayeed, M. N.; Alarfaj, A. *Chem. Phys. Lett.* **2007**, *445*, 325.
(4) Fujishima, A.; Honda, k. *Nature* **1972**, *238*, 37.
(5) Song, L.; Qiu, R. L.; Mo, Y. K.; Zhang, D. D.; Wei, H.; Xiong, Y. *Catal. Commun.* **2007**, *8*, 429.
(6) Asahi, R.; Morikawa, T.; Ohwaki, T.; Aoki, K.; Taga, Y. *Science* **2001**, *293*, 269.
(7) Liu, G.; Zhao, Y. N.; Sun, C. H.; Li, F.; Lu, G. Q.; Cheng, H. M. *Angew. Chem., Int. Ed.* **2008**, *47*, 4516.
(8) Zhang, H.; Zong, R. L.; Zhao, J. C.; Zhu, Y. F. *Environ. Sci. Technol.* **2008**, *42*, 3803.
(9) Li, D.; Dong, W. J.; Sun, S. M.; Shi, Z.; Feng, S. H. *J. Phys. Chem. C* **2008**, *112*, 14878.
(10) Zhang, L.; Djerdj, I.; Cao, M.; Antonietti, M.; Niederberger, M. *Adv. Mater.* **2007**, *19*, 2083.
(11) Liang, H. C.; Li, X. Z. *Appl. Catal., B* **2009**, *86*, 8.
(12) Ishikawa, A.; Takata, T.; Kondo, J. N.; Hara, M.; Kobayashi, H.; Domen, K. *J. Am. Chem. Soc.* **2002**, *124*, 13547.
(13) Kudo, A.; Omori, K.; Kato, H. *J. Am. Chem. Soc.* **1999**, *121*, 11459.
(14) Sayama, K.; Nomura, A.; Arai, T.; Sugita, T.; Abe, R.; Yanagida, M.; Oi, T.; Iwasaki, Y.; Abe, Y.; Sugihara, H. *J. Phys. Chem. B* **2006**, *110*, 11352.
(15) Xue, F.; Li, H. B.; Zhu, Y. C.; Xiong, S. L.; Zhang, X. W.; Wang, T. T.; Liang, X.; Qian, Y. T. *J. Solid. State. Chem.* **2009**, *182*, 1396.
(16) Fujihara, K.; Izumi, S.; Ohno, T.; Matsumura, M. *J. Photochem. Photobiol. A: Chem.* **2000**, *132*, 99.
(17) Li, Y.; Meng, G. W.; Zhang, L. D. *Appl. Phys. Lett.* **2000**, *76*, 2011.
(18) Gao, F.; Chen, X. Y.; Yin, K. B.; Dong, S.; Ren, Z. F.; Yuan, F.; Yu, T.; Zou, Z. G.; Liu, J. M. *Adv. Mater.* **2007**, *19*, 2889.
(19) Jones, C. A.; Stec, D.; Larsen, S. C. *J. Mol. Catal. A: Chem.* **2004**, *212*, 329.
(20) Poisson, S.; d'Yvoire, F.; Nguyen-Huy-Dung.; Bretey, E.; Berthet, P. *J. Solid. State. Chem.* **1998**, *138*, 32.
(21) Chen, D. M.; Yang, D.; Geng, J. Q.; Zhu, J. H.; Jiang, Z. Y. *Appl. Surf. Sci.* **2008**, *225*, 2879.
(22) Chen, B. Y.; Chen, W. M.; Chang, J. S. *J. Hazard. Mater.* **2007**, *139*, 232.
(23) Abe, R.; Sayama, K.; Domen, K.; Arakawa, H. *Chem. Phys. Lett.* **2001**, *344*, 339.
(24) Kuo, C. H.; Chen, C. H.; Huang, M. H. *Adv. Funct. Mater.* **2007**, *17*, 3773.
(25) Ji, G. B.; Tang, S. L.; Ren, S. K.; Zhang, F. M.; Gu, B. X.; Du, Y. W. *J. Cryst. Growth.* **2004**, *270*, 156.
(26) Johnson, C. J.; Dujardin, E.; Davis, S. A.; Murphy, C. J.; Mann, S. *J. Mater. Chem.* **2002**, *12*, 1765.
(27) Lv, Y. Z.; Zhang, Y. H.; Li, C. P.; Ren, L. R.; Guo, L.; Xu, H. B.; Ding, L.; Yang, C. L.; Ge, W. K.; Yang, S. H. *J. Lumin.* **2007**, *122*−*123*, 816.
(28) Lv, Y. Z.; Guo, L.; Xu, H. B.; Ding, L.; Yang, C. L.; Wang, J. N.; Ge, W. K.; Yang, S. H.; Wu, Z. Y. *J. Appl. Phys.* **2006**, *99*, 114302.
(29) Sun, X. M.; Chen, X.; Deng, Z. X.; Li, Y. D. *Mater. Chem. Phys.* **2002**, *78*, 99.
(30) Li, J. X.; Xu, J. H.; Dai, W. L.; Li, H. X.; Fan, K. L. *Appl. Catal., B* **2009**, *85*, 162.
(31) Chen, D. M.; Yang, D.; Geng, J. Q.; Zhu, J. H.; Jiang, Z. Y. *Appl. Surf. Sci.* **2008**, *255*, 2879.
(32) Bang, J. H.; Helmich, R. J.; Suslick, K. S. *Adv. Mater.* **2008**, *20*, 2599.
(33) Tang, J.; Zou, Z.; Ye, J. *J. Phys. Chem. B* **2003**, *107*, 14265.
(34) Sun, S. M.; Wang, W. H.; Zhang, L.; Zhou, L.; Yin, W. Z.; Shang, M. *Environ. Sci. Technol.* **2009**, *43*, 2005.
(35) Lin, P. X.; Huang, F. Q.; Wang, W. D.; Zhang, K. L. *Appl. Catal., A* **2006**, *307*, 257.
(36) Sun, S. M.; Wang, W. Z.; Zhang, L.; Zhou, L.; Yin, W. Z.; Shang, M. *Environ. Sci. Technol.* **2009**, *43*, 2005.
(37) Song, L.; Qiu, R. L.; Mo, Y. Q.; Zhang, D. D.; Wei, H.; Xiong, Y. *Catal. Commun.* **2007**, *8*, 429.
(38) Fa, W. J.; Zan, L.; Gong, C. Q.; Zhong, J. C.; Deng, K. J. *Appl. Catal., B* **2008**, *79*, 216.
(39) Jańczyk, A.; Krakowska, E.; Stochel, G.; Macyk, W. *J. Am. Chem. Soc.* **2006**, *128*, 15574.
(40) Huang, Y. F.; Wei, Y. L.; Fan, L. Q.; Huang, M. L.; Lin, J. M.; Wu, J. H. *Int. J. Hydrogen Energy* **2009**, *34*, 5318.

AM100189M